https://doi.org/10.5194/cp-2023-89
Preprint. Discussion started: 14 November 2023

Climate of the Past
Discussions
Open Access
EGU

Response of Coastal California Hydroclimate to the Paleocene-Eocene Thermal Maximum

Xiaodong Zhang[1*], Brett J. Tipple[2], Jiang Zhu[3], William D. Rush[4], Christian A. Shields[3], Joseph B. Novak[5], James C. Zachos[1]

[1]Department of Earth and Planetary Sciences, University of California, Santa Cruz, CA 95064, USA

[2]FloraTrace Inc., Salt Lake City, UT 84103, USA

[3]Climate and Global Dynamics Laboratory, National Center for Atmospheric Research, Boulder, CO 80307, USA

[4]Department of Environmental Studies and Sciences, Santa Clara University, Santa Clara, CA 95053, USA

[5]Department of Ocean Sciences, University of California, Santa Cruz, CA 95064, USA

**Correspondence to*: Xiaodong Zhang (xzhan335@ucsc.edu)

Abstract. The effects of anthropogenic warming on the hydroclimate of California are becoming more pronounced, with increased frequency of multi-year droughts and flooding. As a past analog for the future, the Paleocene-Eocene Thermal Maximum (PETM) is a unique natural experiment for assessing global and regional hydroclimate sensitivity to greenhouse gas warming. Globally, extensive evidence (i.e., observations, climate models with high pCO_2) demonstrates hydrological intensification with significant variability from region to region (i.e., dryer or wetter, or greater frequency and/or intensity of extreme events). Central California (paleolatitude ~42°N), roughly at the boundary between dry subtropical highs and mid-latitude low pressure systems, would have been particularly susceptible to shifts in atmospheric circulation and precipitation patterns/intensity. Here, we present new observations and climate model output on regional/local hydroclimate responses in central California during PETM. Our findings based on multi-proxy evidence within the context of model output suggest a transition to an overall drier climate punctuated by increased precipitation during summer months along the central coastal California during the PETM.

1 Introduction

Global warming of a few degrees Celsius over the next century is projected to intensify the hydrological cycle on a range of temporal and spatial scales, manifested primarily by amplified wet-dry cycles(Held and Soden, 2006; Douville et al., 2021). Indeed, just over last few decades there has been an increasing frequency in the severity of extremes characterized by compound heat waves and intense drought(Büntgen et al., 2021; Williams et al., 2020; Zscheischler and Lehner, 2022), and/or heavy precipitation and flooding(Liu et al., 2020; Risser and Wehner, 2017). As greenhouse gas driven warming continues, such precipitation extremes (wet or dry) are expected to intensify(Stevenson et al., 2022).

California, a region vulnerable to amplified wet-dry cycles, is already experiencing multiyear extreme droughts with longer precipitation deficits interspersed with anomalously wet years(Zamora-Reyes et al., 2022). For example, the prolonged drought from 2012 to 2016 preceded the exceptionally high numbers of atmospheric river storms-related winter flooding of 2017(Simon Wang et al., 2017). Collectively, climate models (e.g., CESM, CMIP etc.) show that the occurrence of such extremes in droughts and excessive seasonal precipitation in California is expected to increase by the end of the century(Vogel et al., 2020; Swain et al., 2018). In addition, such 'whiplash' hydroclimate shifts related to anthropogenic warming are generally supported by historical records of California climate cycles(de Wet et al., 2021; Polade et al., 2017).

The most robust evidence for greenhouse warming-induced intensification of the hydrological cycle comes from global warming events of the deep past(Carmichael et al., 2017). In particular, the Paleocene-Eocene Thermal Maximum (PETM) has emerged as a unique natural experiment for assessing global and regional hydroclimate sensitivity to greenhouse gas warming(Zachos et al., 2008). Extensive evidence exists for a major mode shift of local/regional precipitation patterns and intensity(Pagani et al., 2006; Slotnick et al., 2012; Schmitz and Pujalte, 2003; Sluijs and Brinkhuis, 2009; Smith et al., 2007; Handley et al., 2012; Kozdon et al., 2020) including enhanced erosion and extreme flooding in fluvial sections (e.g., Pyrenees; Bighorn basin), and increased weathering and sediment fluxes to coastal basins (e.g., Bass River, Wilson Lake, mid-Atlantic coast; Mead Stream, New Zealand etc.) along with other observations(John et al., 2008; Nicolo et al., 2010; Stassen et al., 2012; Self-Trail et al., 2017; Wing et al., 2005; Kraus and Riggins, 2007; Foreman, 2014).

https://doi.org/10.5194/cp-2023-89
Preprint. Discussion started: 14 November 2023

These observations of regional hydroclimate change serve as the basis for climate model experiments forced with proxy-based estimates of ΔpCO_2 for the PETM (i.e., 3x-6x pre-industrial)(Kiehl and Shields, 2013; Carmichael et al., 2016; Zhu et al., 2020). Using such estimates, model simulations show an overall increase in poleward meridional water vapor transport as manifested by a net increase in evaporation of subtropical regions, balanced by higher precipitation of tropical/high latitudes characterizing the 'wet-gets-wetter and dry-gets-drier' hydrological response. The latest simulations using high-resolution climate models display several key regional responses including increased frequency of extreme precipitation events, especially the coastal regions where atmospheric rivers (AR) are common(Rush et al., 2021). Indeed, observations of high-energy flooding events in SW Europe (i.e., the Pyrenees) during the PETM(Schmitz and Pujalte, 2003) can be explained by increased frequency of North Atlantic ARs contributing landfall in that region. Pacific AR activity as simulated for the PETM also becomes more intense but less frequent along the central California coast by shifting northward with the storm tracks(Shields et al., 2021), not unlike the projections for California in the future(Shields and Kiehl, 2016; Massoud et al., 2019). This pattern is consistent with warming scenarios in general which have weakened zonal wind belts (i.e., the westerlies) that are shifting poleward(Abell et al., 2021; Douville et al., 2021).

Testing the theoretical response of Northeast Pacific ARs and seasonal precipitation along North America's western coast in general is challenging and still limited by the lack of observations. Here we constrain the regional hydroclimate response along the central California coast during the PETM using several independent proxies (i.e., clay mineralogy, grain size distribution, $\delta^{13}C_{org}$ stratigraphy, and leaf wax $\delta^2H_{n\text{-alkane}}$ isotope records), which are either directly or indirectly sensitive to shifts in precipitation patterns/intensity. These proxies are then compared against sophisticated Earth System model simulations of the PETM climate to characterize the relative changes in regional precipitation (i.e., pattern/intensity). The new records complement data from a previous study(John et al., 2008), and along with the latest climate modeling experiments provide a unique case study of the sensitivity of regional hydroclimate to major greenhouse warming.

2 Materials and methods

https://doi.org/10.5194/cp-2023-89
Preprint. Discussion started: 14 November 2023

Climate of the Past
Discussions
Open Access

2.1 Site Location

The studied outcrop section is part of the late Paleocene-early Eocene Lodo Formation located in the Panoche Hill of central California (Fig. 1). During the late Paleocene, the section was situated at a paleolatitude ~42°N, roughly at the boundary between the dry subtropical highs and mid-latitude low-pressure systems. The Lodo Formation is comprised primarily of siltstone with a relatively low abundance of calcareous microfossils truncated by thin glauconitic sand layers(Brabb, 1983). Depositional facies are consistent with neritic-bathyal setting along the outer shelf(John et al., 2008).

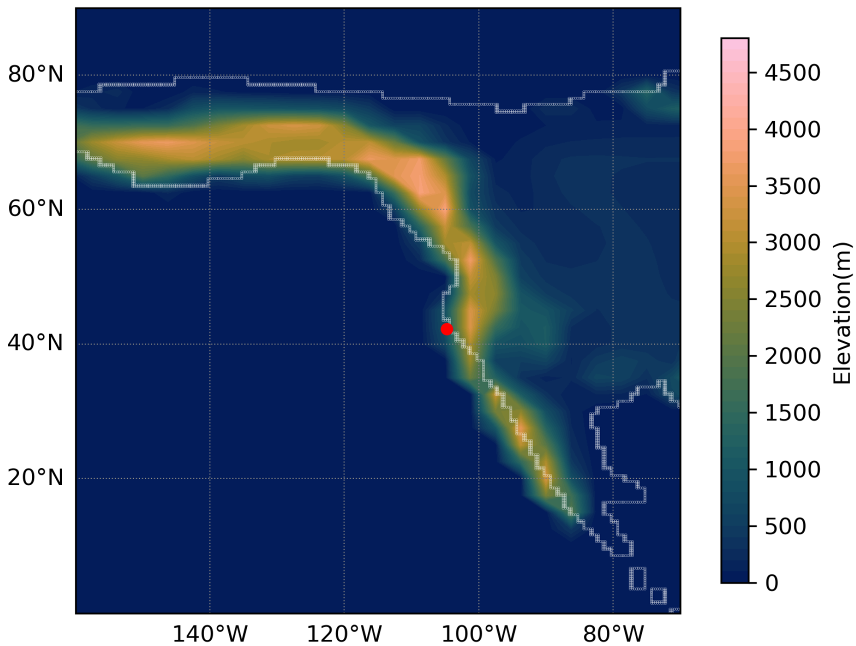

Figure 1. Paleogeography and location of the Lodo Gulch section (red spot) along the Pacific coast at 56 Ma. Late Paleocene-early Eocene topography of North America is adapted from Lunt et al. (2017).

https://doi.org/10.5194/cp-2023-89
Preprint. Discussion started: 14 November 2023

2.2 Methods

2.2.1 Stable isotopes

Sediment samples used for this study include those originally collected by John et al. (2008). In addition, new samples were collected from the upper Paleocene for organic C isotopic analysis to better establish pre-PETM baseline. Samples were analyzed in the UCSC Stable Isotope Laboratory using a CE instruments NC2500 elemental analyzer coupled with Thermo Scientific Delta Plus XP iRMS via a Thermo-Scientific Conflo III. All samples are calibrated with VPDB (Vienna PeeDee Belemnite) for $\delta^{13}C$ and AIR for $\delta^{15}N$ against an in-house gelatin standard reference material (PUGel). Analytical reproducibility precision is ± 0.1 ‰ for $\delta^{13}C$ and ± 0.2 ‰ for $\delta^{15}N$.

2.2.2 Grain Size analysis

Particle size was measured by laser diffraction using Beckman Coulter with Polarization Intensity Differential Scatter (PIDS) housed at UCSC. 2 to 5 mg of bulk sediments was powered in each sample for measurement. Each sample was performed 2 or 3 replicates to ensure reproducibility.

2.2.3 Clay Assemblages analysis

Sample preparation follows a slightly modified version of (Kemp et al., 2016). Roughly 5 to 10 g of sediment was powdered in a pestle and mortar and then placed in a Calgon (Sodium hexametaphosphate) solution on a shaker table for 72 hours. Samples were sorted through a 63 µm sieve while collecting the fluid with the <63 µm fraction. The collected fluid and suspended fine fraction (< 63 µm) were allowed to settle for a period determined by Stokes' Law to keep < 2um size clay particles remaining in suspension. The fluid is then decanted and dried in the oven. Approximately 150 mg clay of each sample is used to prepared oriented mounts for X-ray diffraction (XRD) analysis. A total of 38 clay samples were prepared from the Lodo Formation. The sample residues are measured on a Philips 3040/60 X'pert Pro X-ray diffraction instrument at UCSC. Clay species are identified based on peak positions and intensities representing each clay mineral.

2.2.4 Leaf wax

https://doi.org/10.5194/cp-2023-89
Preprint. Discussion started: 14 November 2023

Sediment extraction, compound isolation, and compound-specific isotope measurements were conducted following Tipple et al., 2011. Briefly, sediments were freeze-dried, powdered (~500 g), and extracted with dichloromethane (DCM): methanol (2:1, v/v) using a Soxhlet extractor. Total lipid extracts were concentrated and then separated by column chromatography using silica gel. Normal-alkanes were further purified from cyclic and branched alkanes using urea adduction following (Wakeham and Pease, 2004). Normal-alkane abundances were determined using gas chromatograph (GC) with a flame ionization detector (FID). Isotope analyses were then performed using a GC coupled to an isotope ratio mass spectrometer interfaced with a GC-C III combustion system or a High Temperature Conversion system for $\delta^{13}C$ and $\delta^{2}H$ analyses, respectively. $\delta^{13}C$ and $\delta^{2}H$ values are expressed relative to Vienna Pee Dee belemnite (VPDB) and Vienna Standard Mean Ocean Water (VSMOW). Individual n-alkane isotope ratios were corrected to n-alkane reference materials (for $\delta^{13}C$, C20, C25, C27, C30, and C38 of known isotopic ratio and for $\delta^{2}H$, "Mix A" from Arndt Schimmelmann, Indiana University) analyzed daily at several concentrations. In addition, H_2 reference gas of known isotopic composition was pulsed between sample n-alkane peaks to confirm if normalizations were appropriate. Standard deviations (SD) of n-alkane reference materials was ±0.6‰ for $\delta^{13}C$ and ±6‰ for $\delta^{2}H$.

2.2.5 Earth System Models

Two different set of climate simulations were used in this paper for (1) comparison with leaf wax proxy data and (2) extreme events analysis. (1) Water isotope-enabled Community Earth System Model version 1.2 (iCESM1.2) simulates changes in climate and water isotopic composition during the PETM (Zhu et al., 2020) with a horizontal resolution of 1.9×2.5° in atmosphere and land, and a nominal 1 degree in the ocean and sea ice components. Water isotope capabilities have been incorporated into all the components of CESM 1.2 (Brady et al., 2019), which include the Community Atmosphere Model, version 5(CAM5) for the atmosphere, the Parellel Ocean Program, version 2(POP2) for the ocean, the Community Land Model, version 4(CLM4) for the land, River Transport Model (RTM) for river flow, and Community Ice Code, version 4 for sea ice. (2) Using the same CESM1.2 framework, high resolution (0.25°) simulations were conducted with forced sea surface temperatures (SSTs) and active atmosphere and land components (CAM5, CLM4). RTM was run at 1° resolution, and forced SST were calculated from consistent 2° fully coupled PETM simulations (see details in Rush et al., 2021 and

https://doi.org/10.5194/cp-2023-89
Preprint. Discussion started: 14 November 2023

reference therein). The much higher horizontal resolution in the atmosphere enables improved simulation of the extreme events. Hourly, daily (CAM5), and monthly(iCESM1.2) temporal resolution precipitation outputs from both sets of climate simulations were utilized in this paper, with 100 years taken from the equilibrated iCESM1.2 simulations, and 15 years from the forced SST high resolution CAM5 simulations.

3 Results

3.1 Carbon isotopes

A carbon isotope excursion is present in both bulk organic and carbonate based $\delta^{13}C$ records across the P-E boundary (Fig. 2a), marking the PETM onset of the Lodo section(John et al., 2008). The terrestrial leaf wax n-alkane record captures the carbon isotope excursion (CIE) with a pattern that roughly parallels the other records. The magnitude of the $\delta^{13}C_{n\text{-alkane}}$ change is roughly 4 ‰ (average of n-C_{27}, n-C_{29}, n-C_{31}) at the onset, followed by a gradual recovery that is truncated marking the top of the PETM body (Fig. 3b).

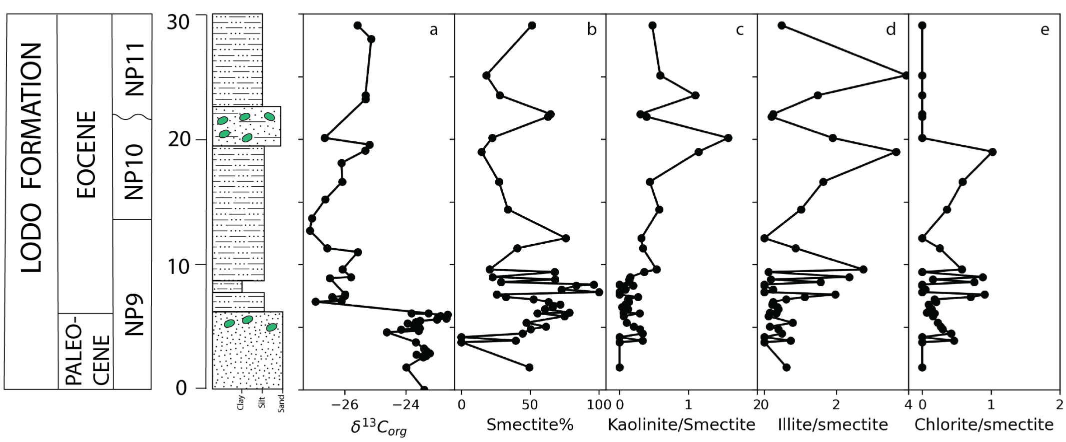

Figure 2. Integrated C isotope and clay assemblage records of Lodo Fm in the Lodo Gulch of central California (a) bulk organic carbon isotope, (b,c,d,e) clay assemblage ratios.

https://doi.org/10.5194/cp-2023-89
Preprint. Discussion started: 14 November 2023

3.2 Hydrogen isotopes

The leaf wax $\delta^2H_{n\text{-alkane}}$ values decrease by 25‰ just prior to the CIE onset followed by a slight enrichment of in the main body PETM (Fig. 3c). The relatively invariable $\delta^2H_{n\text{-alkane}}$ through the PETM is punctuated with one or two brief intervals of more negative values.

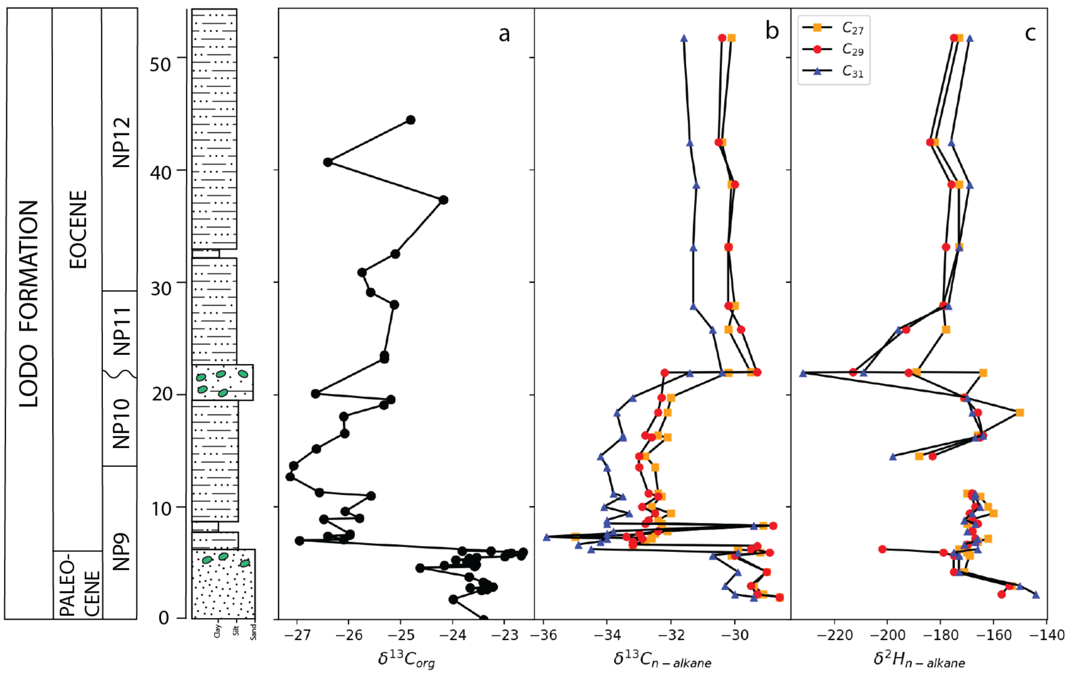

Figure 3. Marine $\delta^{13}C$ and terrestrial higher plant leaf wax n-alkane $\delta^{13}C$ and δ^2H records. (a) bulk organic carbon isotope record of Lodo Fm. (b,c) leaf wax compound specific carbon/hydrogen isotope records in n-C_{27}(yellow), n-C_{29}(red), n-C_{31}(blue).

3.3 Clay Assemblage and grain Size

Clay assemblage data (Fig. 2) shows smectite dominated in the Lodo Formation during PETM, along with increasing illlite/smectite and chlorite/smectite ratios. The lower Lodo Formation, with relative coarse sandy size, shows slight spikes of kaolinite associated with other minerals. Grain size, largely silt and clay, shows a distinct shift toward finer fractions (i.e., clay) with the onset of the CIE (Fig. S1).

https://doi.org/10.5194/cp-2023-89
Preprint. Discussion started: 14 November 2023

3.4 Earth system model simulations

Precipitation output from two earth system models: isotope enabled iCESM1.2 under enhanced greenhouse gas simulations (1x,3x,6x,9x pCO$_2$ pre-industrial) and high-resolution CAM5 models (daily precipitation over 15 years), were analyzed. For this study we used 3x to 6x pCO$_2$ forcing that best replicate the observed ΔSST from pre-PETM to PETM(Zhu et al., 2020). Overall, monthly precipitation for the study region decreases during the PETM in both simulations but with a slight increase in the summer (Fig. 4,5). CAM5 output shows a modest decrease in mean annual precipitation with significant seasonal shifts during PETM (Fig. 5a). Seasonal changes of monthly averaged δ^{18}O and δ^{2}H from mean monthly precipitation (MAP) in iCESM1.2 of central California are consistent with CAM5. On average the δ^{2}H increases by ca. 10 ‰ from pre-PETM to PETM, especially in the winter/spring, with a smaller shift in summer/fall (Fig 4. a,b,c). The Extreme value index (ξ), a representation of the distribution of exceedance right tail (supplemental information), shows a small but statistically robust increase in wet extremes of winter (DJF) with a significant increase in summer (JJA) wet exceedances during the PETM in the precipitation output from CAM5 simulations (Fig. 5b).

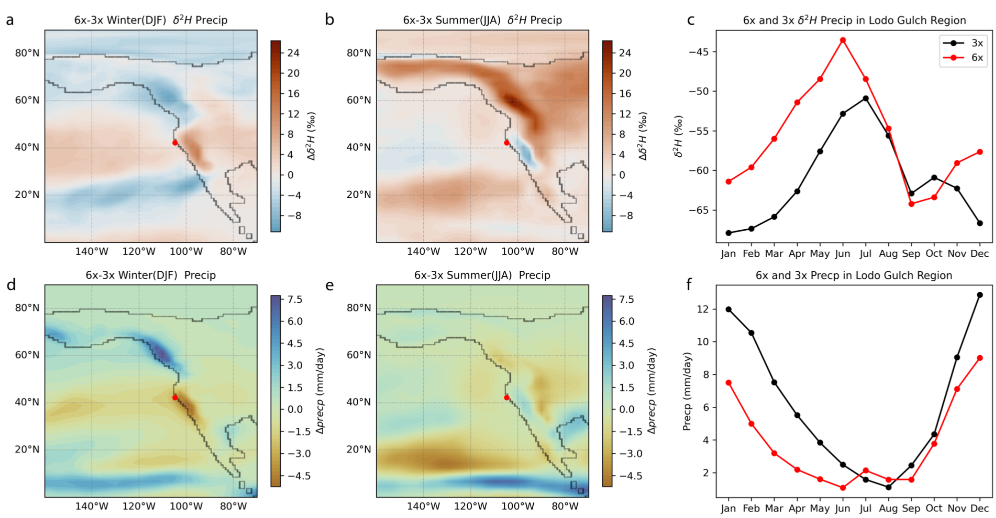

Figure 4. Water isotope-enable iCESM1.2 model output (Zhu et al., 2020) of monthly hydrogen isotope record of meteoric precipitation under different pCO$_2$ forcing to pre-industry (3x in black

represents pre-PETM, 6x in red represents PETM) in east Pacific coast (red spot represents the Lodo Gulch study site). The iCESM1.2 simulations used the DeepMIP boundary conditions (Lunt et al., 2017). Difference in winter (a) and summer (b) hydrogen isotope composition between pre-PETM(3x) and PETM(6x). (c) Annual seasonal cycle of hydrogen isotope composition of precipitation in Lodo Gulch region. Difference in winter(d) and summer(e) precipitation amount between pre-PETM(3x) and PETM(6x) in east Pacific coast. (f) Annual seasonal cycle of precipitation amount in Lodo Gulch region. Site values of Lodo Gulch region are calculated by area-weighted average over 4° x 4° box around study site.

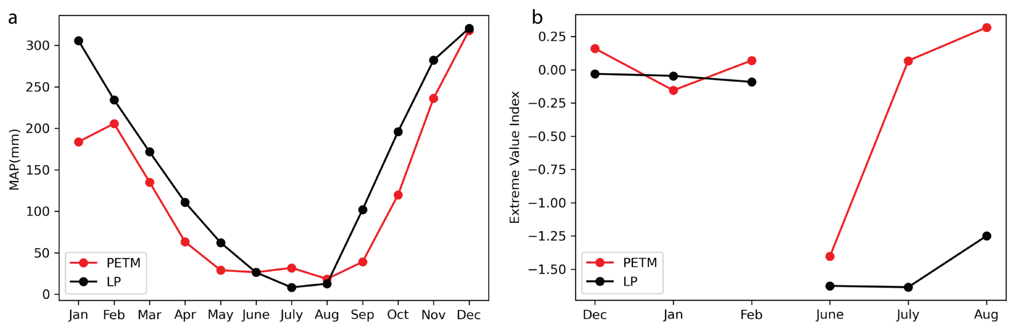

Figure 5. (a) High resolution CAM5 model output of mean monthly precipitation over 15 model years in central coastal California regions during pre-PETM (Late Paleocene/LP) under low pCO_2 (680 ppmv) and PETM under high pCO_2 (1590ppmv). (b) Extreme value index (ξ) results of mean monthly precipitation in winter versus summer of central coastal California region.

4 Discussion

Independent proxies (i.e, sediment flux, clay assemblages, and water isotopes ($^2H/^1H$ or $^{18}O/^{16}O$), though each has limitations, collectively can contribute toward a general picture of how the mode of precipitation changed (i.e., wetter or dryer, and/or greater seasonality or extremes). For central California, model simulations of the PETM with low and high resolutions exhibit an overall decrease in mean annual precipitation (Fig. 4,5). For a mountainous coastal environment (Fig. 1), siliciclastic sedimentation rates should be highly susceptible to hydrologic changes among other factors. In addition to relief and lithology, the seasonality of precipitation and vegetation cover would be major controls on erosion and siliciclastic sediment fluxes. However, constraining sedimentation rates in shelf sections is challenging given the limitations of

https://doi.org/10.5194/cp-2023-89
Preprint. Discussion started: 14 November 2023

chronostratigraphy in such facies. As such, we rely largely on biostratigraphic constraints with carbon isotope stratigraphy as the CIE is well captured in both organic and inorganic (calcite) fossil materials in Lodo (John et al., 2008). This expanded CIE interval indicates higher sedimentation rates during the PETM (John et al., 2008). Sedimentation rates on the continental shelf margin are highly sensitive to terrestrial sediment discharge and relative sea-level change. Assuming the latter was relatively static or rising (Sluijs et al., 2008), the higher sedimentation rates suggest increasing sediment supply from river runoff to the continental margin, reflecting a mode shift in regional hydroclimate.

4.1 Hydroclimate response from clay mineralogy

Clay assemblages in nearshore settings can reflect physical and chemical weathering changes as influenced by regional climate change. Indeed, an increase in the relative abundance of kaolinite fluxes has been widely observed across the CIE onset in many PETM sections from mid to high latitudes(Tateo, 2020; Gibson et al., 2000) and interpreted as evidence of a major mode shift in local hydroclimates. In contrast, the clay mineralogy (Fig. 3) for the Lodo Formation is dominated mainly by smectite at the onset of the PETM, consistent with seasonal wet/dry cycles under warm conditions(Gibson et al., 2000). A subtle increase in the kaolinite/smectite hints slightly enhanced humidity, possibly related to enhanced seasonally subtropical conditions(Foreman, 2014). Such inferences of hydroclimate changes in the context of coastal deposition are complicated by fluvial runoff conditions (i.e., provenance, discharge, sediment influx) and precipitation (i.e., seasonal vs mean annual). Skewed grain size distribution of clay sediments coinciding with illite/kaolinite peaks (Fig. S1) indicates higher fluvial velocity and increased erosion as observed in other locations(Chen et al., 2018; Foreman et al., 2012; Foreman, 2014). The lower Lodo Formation, with relative coarse sandy size distribution preceding the PETM, shows a slight pulse of kaolinite associated with other minerals, possibly indicating an early change of hydrological condition in the latest Paleocene before the PETM as observed elsewhere (Rush et al., 2021). The CIE onset likely represents a transient response to warming-induced hydroclimate changes, whereas the pre-PETM shift as well as minor variations post-CIE onset are likely orbitally forced (Kiehl et al., 2018).

4.2 Hydroclimate response from earth system simulations

https://doi.org/10.5194/cp-2023-89
Preprint. Discussion started: 14 November 2023

In all model simulations forced with higher pCO2 (e.g., 3x to 6x pre-industrial), the hydrological cycle during PETM intensifies as manifested by increases in global mean precipitation and meridional vapor transport (Kiehl and Shields, 2013; Kiehl et al., 2018; Carmichael et al., 2016; Zhu et al., 2020). Regionally however, the magnitude and even the sign of precipitation change can differ considerably from global means. This is most evident in the latest low and high-resolution model simulations of the PETM. For central California, the simulations yield modest changes in mean annual precipitation but significant seasonal shifts with a notable decline in winter precipitation and a slight increase in summer (Fig. 4). This pattern is produced by both the water isotope enabled iCESM1.2 and the higher resolution CAM5 with an overall shift into lower amplitude seasonal cycles as a drier winter/spring and a slightly wetter summer (Fig. 4, 5). This seasonal wet-dry shift appears to be driven in part by a pronounced northward shift of atmospheric rivers (ARs) in winter along the Pacific coast(Shields et al., 2021). Given the ARs delivering the majority of winter precipitation to the mid-latitude Pacific coast, less frequent AR occurrences would result in relatively drier winters during PETM. Moreover, the extreme value index (ξ) shows a small but statistically robust increase winter (DF) wet extremes with a significant increase in the probability of summer (JJA) wet exceedance during PETM (Fig. 5b). Although AR related coastal winter storms reduced in frequency (Shields et al., 2021), summer precipitation increased in intensity thus potentially enhancing individual extremes in this region, possibly related to an increase in summer tropical storm activity along the Pacific coast during PETM (Fig. S4).

4.3 $^2H/^1H$ composition of leaf waxes.

Terrestrial archives exhibit considerable evidence of environmental response to intensified hydrological cycle during the PETM (McInerney and Wing, 2011). In western North America, plant fossils show widely expansion (up to 40°N) of tropical rainforest during the PETM along the east Pacific in mid-latitude(Willis, K.J, McElwain, 2002; Korasidis et al., 2022). Terrestrial higher plant hydrogen isotope composition (i.e., $\delta^2H_{n\text{-alkane}}$) provide evidence for regional mode shifts of precipitation (Handley et al., 2008, 2011; Jaramillo et al., 2010; Pagani et al., 2006; Tipple et al., 2011). Generally, δ^2H significantly increases in most of these records as expected with warming, but regionally, notable similarities and differences existed. In subtropical/mid-latitude regions, δ^2H increases prior to the PETM followed by a large negative excursion (ca ~20‰) across the onset of PETM (Handley et al., 2008, 2011; Jaramillo et al., 2010; Tipple et

https://doi.org/10.5194/cp-2023-89
Preprint. Discussion started: 14 November 2023

al., 2011). In sharp contrast, high latitudes $\delta^2H_{n\text{-alkane}}$ show a positive excursion of 55‰ at CIE onset during PETM, consistent with a reduced meridional temperature gradient and decreasing isotope distillation during vapor transport (Pagani et al., 2006). However, the Lodo $\delta^2H_{n\text{-alkane}}$ displays a comparatively muted response, initially decreasing by 25‰ just prior to the CIE onset followed by a slight ^2H enrichment in the main body PETM followed by several shifts toward more negative values (Fig. 3c). The shift to more negative $\delta^2H_{n\text{-alkane}}$ values prior to the onset of CIE in Lodo likely represents background variability related to orbital forcing.

Inferring and comparing the hydroclimate response from leaf water δ^2H at any location can be complicated. Hydrogen isotope fractionation in plants is tightly related to photosynthetic pathways, source water availability, and atmospheric humidity (Sachse et al., 2012; Tipple et al., 2015). Along the west coast of North America, no detailed records of vegetation response have been generated for the PETM. Lack of knowledge about vegetation changes limits our ability to compute rainwater δ^2H. Further, under higher weathering rates during the PETM, deep weathering of Paleocene n-alkanes (Tipple et al., 2011) would possibly dampen of isotopic n-alkane signals deposited at Lodo. Nevertheless, if we assume the $\delta^2H_{n\text{-alkane}}$ record reflects only on changes in source water, the observed modest change of $\delta^2H_{n\text{-alkane}}$ values at Lodo could be interpreted in several ways with respect to T-related changes on isotope fractionation offset by changes in dominant season of precipitation, and/or vapor sources and distance of transport. For example, a shift in precipitation seasonally between winter and late summer/fall could offset the effects of warming assuming a shift from a proximal (north or central Pacific) to a more distal (Gulf of Mexico) source of vapor (Hu and Dominguez, 2015). At ground level, stronger evapotranspiration during biosynthesis can isotopically be offset by external water source availability (i.e. seasonal precipitation). Local/regional ground water table variations caused by hydrological change would also affect the source water-use efficiency of plants since surface water tends to be more depleted in some perennial species after intense storms in the groundwater (Hou et al., 2008; Krishnan et al., 2014). Hydrogen isotope fractionation in plants can also be biased by seasonal shift in regional vegetation growth regime. For example, leaf wax lipids from terrestrial plants usually record hydrological conditions earlier in the season rather than fully integrating the entire growing season (Hou et al., 2008; Tipple et al., 2013). Finally, episodic extremes in precipitation may dominate the hydrogen isotopic composition of the leaf wax (Krishnan et al., 2014). If most soil water from extreme events during the growth season, the

https://doi.org/10.5194/cp-2023-89
Preprint. Discussion started: 14 November 2023

Lodo $\delta^2H_{n\text{-alkane}}$ changes might reflect a combination effect of intensified seasonal storms with more ^{2}H-depleted precipitation offset by warming induced ^{2}H-enrichment in leaf water.

In iCESM1.2 simulations with increasing pCO$_2$ (i.e., 3x to 6x pre-industry) and SST, the seasonal shifts in δ^2H of mean monthly precipitation from pre-PETM to PETM is significant. Regional δ^2H_{precp} increases by 10‰ during wet winter while decreasing by ~1 to 5‰ during late summer/fall in central California (Fig. 4). To estimate how this seasonal change of δ^2H_{precp} and precipitation amount influences leaf water δ^2H, we apply a leaf wax proxy model (supplemental information) which computes the combined effects of changes in seasonal precipitation and growing season length. The model shows leaf water δ^2H enriched ca. 4 to 7‰ from pre-PETM to PETM consistent with $\delta^2H_{n\text{-alkane}}$ proxy record in Lodo section. Therefore, this relative muted leaf wax $\delta^2H_{n\text{-alkane}}$ response can be potentially explained by a seasonal shift of heavy precipitation events. Alternatively, the change in leaf water δ^2H may also reflect source water shift of a mixing endmember between proximal and distal sources of water in the coast (Romero and Feakins, 2011). For example, with a summer shift of source water from the Pacific to subtropics (i.e., summer monsoons), the effect of increasing distance and distillation would isotopically deplete vapor (Hu and Dominguez, 2015), thus offsetting the temperature related enrichment of local δ^2H_{precip}. Infrequent but high intensity tropical cyclones-induced heavy rainfall in the summer in mid-Pacific during PETM (Kiehl et al., 2021) can also bring the precipitation more depleted in hydrogen isotope (i.e., a more negative δ^2H).

Finally, a related record that might indirectly reflect on precipitation amount (i.e., atmospheric humidity) is the n-alkane δ^{13}C and magnitude of the CIE. Recalcitrant higher plants leaf wax carbon isotope ratios of long-chain n-alkane (n>25 with odd-over-even preference) reflect mainly carbon source (Diefendorf et al., 2010). However, photosynthetic carbon isotope fractionation (Δ_p) is sensitive to atmospheric pCO$_2$ variations, generally increase with rising concentrations assuming a constant photosynthetic fractionation factor and humidity (Diefendorf et al., 2010). The $\delta^{13}C_{n\text{-alkane}}$ of Lodo section displays a sharp negative shift of ca. 4 ‰ (average of n-C$_{27}$, n-C$_{29}$, n-C$_{31}$) across the onset of CIE (Fig. 3b), which is consistent with global mean atmospheric CIE (Sluijs and Dickens, 2012) but generally smaller than observed in other leaf wax records (Handley et al., 2008, 2011; Jaramillo et al., 2010; Pagani et al., 2006; Tipple et al., 2011). The smaller $\delta^{13}C_{n\text{-alkane}}$ CIE recorded in Lodo could reflect on reduction in local humidity which preferentially tends to reduce the magnitude of Δ_p during photosynthetic carbon fixation.

5 Conclusion

With PETM greenhouse gas forcing (~56 Ma), climate simulations show an overall decrease in winter precipitation along the central California margin due in part to a reduction in AR frequency(Shields et al., 2021), whereas summer precipitation increases slightly. This is generally consistent with the observations from Lodo Gulch Section based on various sedimentological and geochemical records, and thus would support a modest reduction in precipitation (i.e. MAP) along with the possibility of an increase magnitude of extreme precipitation events during the PETM. In this regard, the observed hydroclimate response during the PETM as simulated in climate models in response to a doubling (or more) of CO_2 could serve as a past analog for potential hydroclimate changes in California.

Data availability. Data will be available via the PANGAEA repository.

Author contribution. JCZ conceived the project idea, acquired funding and provided overall supervision. XZ, BJT, WDR, JBN conducted experiments and analyzed the results. JZ, CAS provide technical expertise in model simulations. All authors contributed to the review and editing of the manuscript.

Competing interests. The authors declare that they have no conflict of interest.

Acknowledgements.
Funding for this project has been provided by National Science Foundation No. OCE 2103513. All compound specific isotope analyses were performed at the Yale Institute for Biospheric Studies-Earth Systems Center for Stable Isotopic Studies that was supported by National Science Foundation Grant EAR 0628358 and OCE 0902993. The CESM project is supported primarily by the National Science Foundation (NSF). This material is based upon work supported by the National Center for Atmospheric Research, which is a major facility sponsored by the NSF under Cooperative Agreement No. 1852977.

https://doi.org/10.5194/cp-2023-89
Preprint. Discussion started: 14 November 2023

Reference:

Abell, J. T., Winckler, G., Anderson, R. F., and Herbert, T. D.: Poleward and weakened westerlies during Pliocene warmth, Nature, 589, 70–75, https://doi.org/10.1038/s41586-020-03062-1, 2021.

Brabb, E. E.: Studies in Tertiary stratigraphy of the California Coast Ranges., US Geological Survey Professional Paper, 1213, 1983.

Brady, E., Stevenson, S., Bailey, D., Liu, Z., Noone, D., Nusbaumer, J., Otto-Bliesner, B. L., Tabor, C., Tomas, R., Wong, T., Zhang, J., and Zhu, J.: The Connected Isotopic Water Cycle in the Community Earth System Model Version 1, J Adv Model Earth Syst, 11, 2547–2566, https://doi.org/10.1029/2019MS001663, 2019.

Büntgen, U., Urban, O., Krusic, P. J., Rybníček, M., Kolář, T., Kyncl, T., Ač, A., Koňasová, E., Čáslavský, J., Esper, J., Wagner, S., Saurer, M., Tegel, W., Dobrovolný, P., Cherubini, P., Reinig, F., and Trnka, M.: Recent European drought extremes beyond Common Era background variability, Nat Geosci, 14, 190–196, https://doi.org/10.1038/s41561-021-00698-0, 2021.

Carmichael, M. J., Lunt, D. J., Huber, M., Heinemann, M., Kiehl, J., LeGrande, A., Loptson, C. A., Roberts, C. D., Sagoo, N., Shields, C., Valdes, P. J., Winguth, A., Winguth, C., and Pancost, R. D.: A model-model and data-model comparison for the early Eocene hydrological cycle, Climate of the Past, 12, 455–481, https://doi.org/10.5194/CP-12-455-2016, 2016.

Carmichael, M. J., Inglis, G. N., Badger, M. P. S., Naafs, B. D. A., Behrooz, L., Remmelzwaal, S., Monteiro, F. M., Rohrssen, M., Farnsworth, A., Buss, H. L., Dickson, A. J., Valdes, P. J., Lunt, D. J., and Pancost, R. D.: Hydrological and associated biogeochemical consequences of rapid global warming during the Paleocene-Eocene Thermal Maximum, https://doi.org/10.1016/j.gloplacha.2017.07.014, 1 October 2017.

Chen, C., Guerit, L., Foreman, B. Z., Hassenruck-Gudipati, H. J., Adatte, T., Honegger, L., Perret, M., Sluijs, A., and Castelltort, S.: Estimating regional flood discharge during Palaeocene-Eocene global warming, Sci Rep, 8, 1–8, https://doi.org/10.1038/s41598-018-31076-3, 2018.

Diefendorf, A. F., Mueller, K. E., Wing, S. L., Koch, P. L., and Freeman, K. H.: Global patterns in leaf 13C discrimination and implications for studies of past and future climate, Proc Natl Acad Sci U S A, 107, 5738–5743, https://doi.org/10.1073/pnas.0910513107, 2010.

Douville, H., Raghavan, K., Renwick, J., and Allan, R.: Water Cycle Changes, Intergovernmental Panel on Climate Change 2021 – The Physical Science Basis, 1055–1210, https://doi.org/10.1017/9781009157896.010, 2021.

Foreman, B. Z.: Climate-driven generation of a fluvial sheet sand body at the Paleocene–Eocene boundary in north-west Wyoming (USA), Basin Research, 26, 225–241, https://doi.org/10.1111/BRE.12027, 2014.

Foreman, B. Z., Heller, P. L., and Clementz, M. T.: Fluvial response to abrupt global warming at the Palaeocene/Eocene boundary, Nature 2012 491:7422, 491, 92–95, https://doi.org/10.1038/nature11513, 2012.

Gibson, T. G., Bybell, L. M., and Mason, D. B.: Stratigraphic and climatic implications of clay mineral changes around the Paleocene/Eocene boundary of the northeastern US margin, Sediment Geol, 134, 65–92, https://doi.org/10.1016/S0037-0738(00)00014-2, 2000.

Handley, L., Pearson, P. N., McMillan, I. K., and Pancost, R. D.: Large terrestrial and marine carbon and hydrogen isotope excursions in a new Paleocene/Eocene boundary section from Tanzania, Earth Planet Sci Lett, 275, 17–25, https://doi.org/10.1016/j.epsl.2008.07.030, 2008.

https://doi.org/10.5194/cp-2023-89
Preprint. Discussion started: 14 November 2023

Handley, L., Crouch, E. M., and Pancost, R. D.: A New Zealand record of sea level rise and environmental change during the Paleocene-Eocene Thermal Maximum, Palaeogeogr Palaeoclimatol Palaeoecol, 305, 185–200, https://doi.org/10.1016/j.palaeo.2011.03.001, 2011.

Handley, L., O'Halloran, A., Pearson, P. N., Hawkins, E., Nicholas, C. J., Schouten, S., McMillan, I. K., and Pancost, R. D.: Changes in the hydrological cycle in tropical East Africa during the Paleocene-Eocene Thermal Maximum, Palaeogeogr Palaeoclimatol Palaeoecol, 329–330, 10–21, https://doi.org/10.1016/j.palaeo.2012.02.002, 2012.

Held, I. M. and Soden, B. J.: Robust Responses of the Hydrological Cycle to Global Warming, J Clim, 19, 5686–5699, https://doi.org/10.1175/JCLI3990.1, 2006.

Hou, J., D'Andrea, W. J., and Huang, Y.: Can sedimentary leaf waxes record D/H ratios of continental precipitation? Field, model, and experimental assessments, Geochim Cosmochim Acta, 72, 3503–3517, https://doi.org/10.1016/j.gca.2008.04.030, 2008.

Hu, H. and Dominguez, F.: Evaluation of Oceanic and Terrestrial Sources of Moisture for the North American Monsoon Using Numerical Models and Precipitation Stable Isotopes, J Hydrometeorol, 16, 19–35, https://doi.org/10.1175/JHM-D-14-0073.1, 2015.

Jaramillo, C., Ochoa, D., Contreras, L., Pagani, M., Carvajal-Ortiz, H., Pratt, L. M., Krishnan, S., Cardona, A., Romero, M., Quiroz, L., Rodriguez, G., Rueda, M. J., De La Parra, F., Morón, S., Green, W., Bayona, G., Montes, C., Quintero, O., Ramirez, R., Mora, G., Schouten, S., Bermudez, H., Navarrete, R., Parra, F., Alvarán, M., Osorno, J., Crowley, J. L., Valencia, V., and Vervoort, J.: Effects of rapid global warming at the paleocene-eocene boundary on neotropical vegetation, Science (1979), 330, 957–961, https://doi.org/10.1126/science.1193833, 2010.

John, C. M., Bohaty, S. M., Zachos, J. C., Sluijs, A., Gibbs, S., Brinkhuis, H., and Bralower, T. J.: North American continental margin records of the Paleocene-Eocene thermal maximum: Implications for global carbon and hydrological cycling, Paleoceanography, 23, https://doi.org/10.1029/2007PA001465, 2008.

Kemp, S. J., Ellis, M. A., Mounteney, I., and Kender, S.: Palaeoclimatic implications of high-resolution clay mineral assemblages preceding and across the onset of the Palaeocene–Eocene Thermal Maximum, North Sea Basin, Clay Miner, 51, 793–813, https://doi.org/10.1180/CLAYMIN.2016.051.5.08, 2016.

Kiehl, J. T. and Shields, C. A.: Sensitivity of the palaeocene-eocene thermal maximum climate to cloud properties, Philosophical Transactions of the Royal Society A: Mathematical, Physical and Engineering Sciences, 371, https://doi.org/10.1098/rsta.2013.0093, 2013.

Kiehl, J. T., Shields, C. A., Snyder, M. A., Zachos, J. C., and Rothstein, M.: Greenhouse- and orbital-forced climate extremes during the early Eocene, Philosophical Transactions of the Royal Society A: Mathematical, Physical and Engineering Sciences, 376, https://doi.org/10.1098/RSTA.2017.0085, 2018.

Kiehl, J. T., Zarzycki, C. M., Shields, C. A., and Rothstein, M. V.: Simulated changes to tropical cyclones across the Paleocene-Eocene Thermal Maximum (PETM) boundary, Palaeogeogr Palaeoclimatol Palaeoecol, 572, 110421, https://doi.org/10.1016/J.PALAEO.2021.110421, 2021.

Korasidis, V. A., Wing, S. L., Shields, C. A., and Kiehl, J. T.: Global Changes in Terrestrial Vegetation and Continental Climate During the Paleocene-Eocene Thermal Maximum, Paleoceanogr Paleoclimatol, 37, https://doi.org/10.1029/2021PA004325, 2022.

Kozdon, R., Penman, D. E., Kelly, D. C., Zachos, J. C., Fournelle, J. H., and Valley, J. W.: Enhanced Poleward Flux of Atmospheric Moisture to the Weddell Sea Region (ODP Site 690) During the Paleocene-Eocene Thermal Maximum, Paleoceanogr Paleoclimatol, 35, 1–14, https://doi.org/10.1029/2019pa003811, 2020.

https://doi.org/10.5194/cp-2023-89
Preprint. Discussion started: 14 November 2023

Climate of the Past
Discussions
Open Access

Kraus, M. J. and Riggins, S.: Transient drying during the Paleocene-Eocene Thermal Maximum (PETM): Analysis of paleosols in the bighorn basin, Wyoming, Palaeogeogr Palaeoclimatol Palaeoecol, 245, 444–461, https://doi.org/10.1016/j.palaeo.2006.09.011, 2007.

Krishnan, S., Pagani, M., Huber, M., and Sluijs, A.: High latitude hydrological changes during the Eocene Thermal Maximum 2, Earth Planet Sci Lett, 404, 167–177, https://doi.org/10.1016/j.epsl.2014.07.029, 2014.

Liu, B., Yan, Y., Zhu, C., Ma, S., and Li, J.: Record-Breaking Meiyu Rainfall Around the Yangtze River in 2020 Regulated by the Subseasonal Phase Transition of the North Atlantic Oscillation, Geophys Res Lett, 47, https://doi.org/10.1029/2020GL090342, 2020.

Massoud, E. C., Espinoza, V., Guan, B., and Waliser, D. E.: Global Climate Model Ensemble Approaches for Future Projections of Atmospheric Rivers, Earths Future, 7, 1136–1151, https://doi.org/10.1029/2019EF001249, 2019.

McInerney, F. A. and Wing, S. L.: The Paleocene-Eocene Thermal Maximum: A Perturbation of Carbon Cycle, Climate, and Biosphere with Implications for the Future, Annu Rev Earth Planet Sci, 39, 489–516, https://doi.org/10.1146/annurev-earth-040610-133431, 2011.

Nicolo, M. J., Dickens, G. R., and Hollis, C. J.: South Pacific intermediate water oxygen depletion at the onset of the Paleocene-Eocene thermal maximum as depicted in New Zealand margin sections, Paleoceanography, 25, 1–12, https://doi.org/10.1029/2009PA001904, 2010.

Pagani, M., Pedentchouk, N., Huber, M., Sluijs, A., Schouten, S., Brinkhuis, H., Damsté, J. S. S., Dickens, G. R., Backman, J., Clemens, S., Cronin, T., Eynaud, F., Gattacceca, J., Jakobsson, M., Jordan, R., Kaminski, M., King, J., Koc, N., Martinez, N. C., McInroy, D., Moore, T. C., O'Regan, M., Onodera, J., Pälike, H., Rea, B., Rio, D., Sakamoto, T., Smith, D. C., St John, K. E. K., Suto, I., Suzuki, N., Takahashi, K., Watanabe, M., and Yamamoto, M.: Arctic hydrology during global warming at the Palaeocene/Eocene thermal maximum, Nature, 442, 671–675, https://doi.org/10.1038/nature05043, 2006.

Polade, S. D., Gershunov, A., Cayan, D. R., Dettinger, M. D., and Pierce, D. W.: Precipitation in a warming world: Assessing projected hydro-climate changes in California and other Mediterranean climate regions OPEN, Sci Rep, 7, https://doi.org/10.1038/s41598-017-11285-y, 2017.

Risser, M. D. and Wehner, M. F.: Attributable Human-Induced Changes in the Likelihood and Magnitude of the Observed Extreme Precipitation during Hurricane Harvey, Geophys Res Lett, 44, 12,457-12,464, https://doi.org/10.1002/2017GL075888, 2017.

Romero, I. C. and Feakins, S. J.: Spatial gradients in plant leaf wax D/H across a coastal salt marsh in southern California, Org Geochem, 42, 618–629, https://doi.org/10.1016/J.ORGGEOCHEM.2011.04.001, 2011.

Rush, W. D., Kiehl, J. T., Shields, C. A., and Zachos, J. C.: Increased frequency of extreme precipitation events in the North Atlantic during the PETM: Observations and theory, Palaeogeogr Palaeoclimatol Palaeoecol, 568, https://doi.org/10.1016/j.palaeo.2021.110289, 2021.

Sachse, D., Billault, I., Bowen, G. J., Chikaraishi, Y., Dawson, T. E., Feakins, S. J., Freeman, K. H., Magill, C. R., McInerney, F. A., van der Meer, M. T. J., Polissar, P., Robins, R. J., Sachs, J. P., Schmidt, H.-L., Sessions, A. L., White, J. W. C., West, J. B., and Kahmen, A.: Molecular Paleohydrology: Interpreting the Hydrogen-Isotopic Composition of Lipid Biomarkers from Photosynthesizing Organisms, Annu Rev Earth Planet Sci, 40, 221–249, https://doi.org/10.1146/annurev-earth-042711-105535, 2012.

https://doi.org/10.5194/cp-2023-89
Preprint. Discussion started: 14 November 2023

Schmitz, B. and Pujalte, V.: Sea-level, humidity, and land-erosion records across the initial Eocene thermal maximum from a continental-marine transect in northern Spain, Geology, 31, 689–692, https://doi.org/10.1130/G19527.1, 2003.

Self-Trail, J. M., Robinson, M. M., Bralower, T. J., Sessa, J. A., Hajek, E. A., Kump, L. R., Trampush, S. M., Willard, D. A., Edwards, L. E., Powars, D. S., and Wandless, G. A.: Shallow marine response to global climate change during the Paleocene-Eocene Thermal Maximum, Salisbury Embayment, USA, Paleoceanography, 32, 710–728, https://doi.org/10.1002/2017PA003096, 2017.

Shields, C. A. and Kiehl, J. T.: Atmospheric river landfall-latitude changes in future climate simulations, Geophys Res Lett, 43, 8775–8782, https://doi.org/10.1002/2016GL070470, 2016.

Shields, C. A., Kiehl, J. T., Rush, W., Rothstein, M., and Snyder, M. A.: Atmospheric rivers in high-resolution simulations of the Paleocene Eocene Thermal Maximum (PETM), Palaeogeogr Palaeoclimatol Palaeoecol, 567, https://doi.org/10.1016/j.palaeo.2021.110293, 2021.

Simon Wang, S. Y., Yoon, J. H., Becker, E., and Gillies, R.: California from drought to deluge, Nature Climate Change 2017 7:7, 7, 465–468, https://doi.org/10.1038/nclimate3330, 2017.

Slotnick, B. S., Dickens, G. R., Nicolo, M. J., Hollis, C. J., Crampton, J. S., Zachos, J. C., and Sluijs, A.: Large-amplitude variations in carbon cycling and terrestrial weathering during the latest Paleocene and earliest Eocene: The record at Mead Stream, New Zealand, Journal of Geology, 120, 487–505, https://doi.org/10.1086/666743, 2012.

Sluijs, A. and Brinkhuis, H.: A dynamic climate and ecosystem state during the Paleocene-Eocene Thermal Maximum: Inferences from dinoflagellate cyst assemblages on the New Jersey Shelf, Biogeosciences, 6, 1755–1781, https://doi.org/10.5194/bg-6-1755-2009, 2009.

Sluijs, A. and Dickens, G. R.: Assessing offsets between the δ13C of sedimentary components and the global exogenic carbon pool across early Paleogene carbon cycle perturbations, Global Biogeochem Cycles, 26, https://doi.org/10.1029/2011GB004224, 2012.

Sluijs, A., Brinkhuis, H., Crouch, E. M., John, C. M., Handley, L., Munsterman, D., Bohaty, S. M., Zachos, J. C., Reichart, G. J., Schouten, S., Pancost, R. D., Damsté, J. S. S., Welters, N. L. D., Lotter, A. F., and Dickens, G. R.: Eustatic variations during the Paleocene-Eocene greenhouse world, Paleoceanography, 23, https://doi.org/10.1029/2008PA001615, 2008.

Smith, F. A., Wing, S. L., and Freeman, K. H.: Magnitude of the carbon isotope excursion at the Paleocene-Eocene thermal maximum: The role of plant community change, Earth Planet Sci Lett, 262, 50–65, https://doi.org/10.1016/j.epsl.2007.07.021, 2007.

Stassen, P., Thomas, E., and Speijer, R. P.: The progression of environmental changes during the onset of the Paleocene-Eocene thermal maximum (New Jersey coastal plain), Austrian Journal of Earth Sciences, 105, 169–178, 2012.

Stevenson, S., Coats, S., Touma, D., Cole, J., Lehner, F., Fasullo, J., and Otto-Bliesner, B.: Twenty-first century hydroclimate: A continually changing baseline, with more frequent extremes, PNAS, 119, https://doi.org/10.1073/pnas, 2022.

Swain, D. L., Langenbrunner, B., Neelin, J. D., and Hall, A.: Increasing precipitation volatility in twenty-first-century California, Nat Clim Chang, 8, 427–433, https://doi.org/10.1038/s41558-018-0140-y, 2018.

Tateo, F.: Clay minerals at the paleocene–eocene thermal maximum: Interpretations, limits, and perspectives, Minerals, 10, 1–16, https://doi.org/10.3390/min10121073, 2020.

Tipple, B. J., Pagani, M., Krishnan, S., Dirghangi, S. S., Galeotti, S., Agnini, C., Giusberti, L., and Rio, D.: Coupled high-resolution marine and terrestrial records of carbon and hydrologic cycles

https://doi.org/10.5194/cp-2023-89
Preprint. Discussion started: 14 November 2023

variations during the Paleocene – Eocene Thermal Maximum (PETM), Earth Planet Sci Lett, 311, 82–92, https://doi.org/10.1016/j.epsl.2011.08.045, 2011.
Tipple, B. J., Berke, M. A., Doman, C. E., Khachaturyan, S., and Ehleringer, J. R.: Leaf-wax n-alkanes record the plant-water environment at leaf flush, Proc Natl Acad Sci U S A, 110, 2659–2664, https://doi.org/10.1073/pnas.1213875110, 2013.
Tipple, B. J., Berke, M. A., Hambach, B., Roden, J. S., and Ehleringer, J. R.: Predicting leaf wax n-alkane 2H/1H ratios: controlled water source and humidity experiments with hydroponically grown trees confirm predictions of Craig–Gordon model, Plant Cell Environ, 38, 1035–1047, https://doi.org/10.1111/PCE.12457, 2015.
Vogel, M. M., Hauser, M., and Seneviratne, S. I.: Projected changes in hot, dry and wet extreme events' clusters in CMIP6 multi-model ensemble, Environmental Research Letters, 15, https://doi.org/10.1088/1748-9326/ab90a7, 2020.
Wakeham, S. G. and Pease, T. K.: Lipid Analysis in Marine Particle and Sediment Samples A Laboratory Handbook, 2004.
de Wet, C. B., Erhardt, A. M., Sharp, W. D., Marks, N. E., Bradbury, H. J., Turchyn, A. V., Xu, Y., and Oster, J. L.: Semiquantitative Estimates of Rainfall Variability During the 8.2 kyr Event in California Using Speleothem Calcium Isotope Ratios, https://doi.org/10.1029/2020GL089154, 16 February 2021.
Williams, A. P., Cook, E. R., Smerdon, J. E., Cook, B. I., Abatzoglou, J. T., Bolles, K., Baek, S. H., Badger, A. M., and Livneh, B.: Large contribution from anthropogenic warming to an emerging North American megadrought, Science (1979), 368, 314–318, 2020.
Willis, K.J, McElwain, J. C.: The Evolution of Plants, OUP Oxford, 392 pp., 2002.
Wing, S. L., Harrington, G. J., Smith, F. a, Bloch, J. I., Boyer, D. M., and Freeman, K. H.: Transient Floral Change and rapid global warming at the P/E boundary, Science (1979), 310, 993–996, https://doi.org/10.1126/science.1116913, 2005.
Zachos, J. C., Dickens, G. R., and Zeebe, R. E.: An early Cenozoic perspective on greenhouse warming and carbon-cycle dynamics, Nature, 451, 279–283, https://doi.org/10.1038/nature06588, 2008.
Zamora-Reyes, D., Broadman, E., Bigio, E., Black, B., Meko, D., Woodhouse, C. A., and Trouet, V.: The Unprecedented Character of California's 20th Century Enhanced Hydroclimatic Variability in a 600-Year Context, Geophys Res Lett, 49, https://doi.org/10.1029/2022GL099582, 2022.
Zhu, J., Poulsen, C. J., Otto-Bliesner, B. L., Liu, Z., Brady, E. C., and Noone, D. C.: Simulation of early Eocene water isotopes using an Earth system model and its implication for past climate reconstruction, Earth Planet Sci Lett, 537, 116164, https://doi.org/10.1016/j.epsl.2020.116164, 2020.
Zscheischler, J. and Lehner, F.: Attributing Compound Events to Anthropogenic Climate Change, Bull Am Meteorol Soc, 103, E936–E953, https://doi.org/10.1175/BAMS-D-21-0116.1, 2022.